

100 Proof: HI Observations of 100 Nearby Dwarf Galaxies with the 100-meter Green Bank Telescope

ALEKSANDRA E. NAZAROVA,¹ JOHN M. CANNON,² IGOR D. KARACHENTSEV,¹ DMITRY I. MAKAROV,¹ MAKSIM I. CHAZOV,¹
LILA SCHISGAL,² AND WILLIAM ST. JOHN²

¹*Special Astrophysical Observatory, The Russian Academy of Sciences, Nizhnij Arkhyz, Karachai-Cherkessian Republic 369167, Russia*

²*Physics and Astronomy Department, Macalester College, 1600 Grand Avenue, Saint Paul, MN 55105, USA*

ABSTRACT

We describe the results of observations with the 100 m Robert C. Byrd Green Bank Telescope (GBT) in the HI line of 105 nearby dwarf galaxies, 60 of which were discovered recently in the DESI Legacy Imaging Surveys. Of 105 objects observed, we detected 77 galaxies with the following median parameters: an HI-flux of $0.69 \text{ Jy km s}^{-1}$, a heliocentric velocity of 732 km s^{-1} , and a W_{50} line width of 32 km s^{-1} . 70 are isolated late-type objects and 35 are new probable satellites of nearby spiral galaxies (NGC 628, NGC 2787, NGC 3556, NGC 4490, NGC 4594 and NGC 5055). The detected galaxies are predominantly gas-rich systems with a median gas-to-stellar-mass ratio of 1.87. In general, they follow the classic Tully-Fisher relation obtained for large disk-dominated spiral galaxies if their M_{21} magnitudes are used instead of B-magnitudes.

Keywords: galaxies: dwarf — galaxies: irregular — galaxies: distances and redshifts

1. INTRODUCTION

Most existing galaxy catalogs are samples, limited by an apparent magnitude or flux of objects in a fixed spectral range. However, the results of modeling the large-scale structure of the Universe within the framework of the standard cosmological model Λ CDM need to be compared with an ensemble of galaxies limited to a fixed volume. The most suitable sample of this type is the Updated Nearby Galaxy Catalog (UNGC, Karachentsev et al. 2013), a regularly updated version¹ of which contains about 1500 galaxies with distances $D < 12 \text{ Mpc}$. It is obvious that the population of this Local Volume (LV) sample can either increase with the advent of deeper sky surveys, or decrease somewhat as the distances of galaxies are refined. The radius of the LV sphere, $\sim 12 \text{ Mpc}$, is defined by the ability to measure the distance of an individual galaxy with an error of 5% using the Tip of the Red Giant Branch (TRGB, Lee et al. 1993; Anand et al. 2020) method in a single-orbit observation with the Hubble Space Telescope (HST). A great advantage of the UNGC catalog is its predominance of low-luminosity

dwarf galaxies, which are usually inaccessible to observations at larger distances. The wealth of observational data on the radial velocities and distances of LV galaxies provides the opportunity to study the local field of peculiar velocities, which is determined by the position and masses of local attractors (i.e., it traces the dark matter distribution on small cosmic scales).

An effective way to gather information about the radial velocities of LV galaxies is via “blind” surveys of large areas of the sky in the 21-cm hydrogen line, such as HIPASS (Koribalski et al. 2004) and ALFALFA (Haynes et al. 2018). These surveys predominantly studied regions with declination $\text{Dec} < +38^\circ$. More northerly coverage is provided by the WSRT HI survey of the Canes Venatici region (Kovač et al. 2009), by the FAST radio telescope (Jiang et al. 2020; Zhang et al. 2024) and by the Apertif Shallow HI Survey (Šiljeg et al. 2024; Adams et al. 2022).

An additional opportunity to detect dwarf galaxies in the LV appeared with the publication of DESI Legacy Imaging Surveys (Dey et al. 2019). The search for new LV objects (Karachentsev & Kaisina 2022; Karachentseva et al. 2023; Karachentsev et al. 2024a) led to the discovery of more than a hundred dwarf galaxies at high declination. About half of them are dwarf spheroidal systems (dSph) with a low content of neutral hydrogen. After excluding dSphs, we selected 54 dwarf galax-

Corresponding author: Aleksandra E. Nazarova
a.e.nazarova@sao.ru

¹ <http://www.sao.ru/lv/lvgdb>

ies with evidence of active star formation to measure their radial velocities with the Green Bank Telescope (GBT). We also added to this sample 51 galaxies from the LV that had no HI-parameter estimates. During the implementation of our program, new HI data from the FASHI survey appeared (Zhang et al. 2024; Karachentsev et al. 2024b). Comparison of these independent data makes it possible to estimate the measurement accuracy of the radial velocity and other parameters of the observed galaxies.

Our article is organized as follows. Section 2 contains a description of observations at the GBT. Section 3 presents the results of observations of our targets in the HI line. Section 4 briefly describes the individual features of the observed galaxies and their environment. Section 5 contains a discussion of the results obtained in the context of the characteristics of other LV late-type dwarf galaxies. Conclusions are presented in Section 6.

2. GBT OBSERVATIONS OF THE NEARBY DWARFS.

We observed 105 dwarf galaxies with the National Radio Astronomy Observatory 100m Robert C. Byrd Green Bank Telescope (GBT²) under projects GBT/23B-032 (P.I. Cannon) and GBT/24B-157 (P.I. Nazarova) with the VEGAS (Versatile GBT Astronomical Spectrometer) backend. ON-OFF position switching observations were performed for all sources; 32,768 channels covered a 23.44 MHz bandpass that was centered at 1410.93 MHz (the rest frequency of HI redshifted by 2000 km s^{-1}). The total effective frequency coverage was from $\sim 1399.2 \text{ MHz}$ to $\sim 1422.6 \text{ MHz}$. This covers the approximate velocity range from -470 to $+4470 \text{ km s}^{-1}$, which is adequate to probe the LV within 10 Mpc. RFI was minimal in the frequency range of interest. Velocities are presented in the optical convention *cz*. Data were acquired during 30 observing sessions in the second half of 2023 and 2024 (100 hours in total). The time per target was typically 40 minutes, 20 minutes of which was spent at the ON-position. The duration could vary markedly depending on the HI brightness.

All reductions were performed in the IDL environment³, using the GBTIDL package designed at NRAO. For most galaxies, velocity and width measurements, along with their errors, were obtained by fitting a single

gaussian to the line profile using the *fitgauss* procedure after fitting and subtracting the local continuum. The resulting spectra have an median rms noise of 3.3 mJy after smoothing to a velocity resolution of 1.81 km s^{-1} using a *boxcar* function. The total flux in the line is calculated as the area under the profile using the *stats* procedure. The corresponding flux error was estimated as the total variance of the background fluctuations. This is true in the case of low flux integrals compared to the background, which is realized in our observations. In two cases, Dw 1247-0824 and Dw 1459+44, there was a double horn line and measurements were taken using the *gmeasure* procedure. For KUG 1033+414 this *gmeasure*-approach resulted in large measurement errors, so the entry in Table 1 contains data for a single gaussian fit.

3. OBSERVATIONAL RESULTS.

Of the 105 GBT targets, the HI signal was detected in 77 dwarf galaxies. Their list is presented in Table 1, whose columns contain the following: (1) the name of the galaxy as indicated in the UNGC (Karachentsev et al. 2013); (2) equatorial coordinates for the epoch J2000.0; (3) apparent optical axial ratio of the galaxy; (4,5) the integral apparent magnitudes in the *B* and *V* bands estimated from *g* magnitude and (*g* - *r*) color, which were measured by us using the DESI Legacy Imaging Surveys⁴ (Dey et al. 2019) images and the transformation equations from The Dark Energy Survey (DESI, Abbott et al. 2021), and in several cases *B* magnitudes were taken from the database HyperLEDA (Makarov et al. 2014); (6) heliocentric radial velocity of the galaxy (km s^{-1}) with indication of its error; (7) full width half maximum of HI line (km s^{-1}) with indication of its error; (8) integral flux in the HI line (Jy km s^{-1}) with indication of its error; (9) kinematic distance of the galaxy in Mpc, calculated via its radial velocity with account of local streams according to the Numerical Action Method model (NAM, Shaya et al. 2017; Kourkchi et al. 2020); (10,11) hydrogen and stellar mass (in solar masses) determined in Section 5.

The $2' \times 2'$ images (North up and East to the left) from the DESI Legacy Imaging Surveys of the 77 detected sources are presented in Fig. 1. Their spectra are shown in Fig. 2. Insets in each panel provide S_{HI} and W_{50} values.

² The National Radio Astronomy Observatory and Green Bank Observatory are facilities of the U.S. National Science Foundation operated under cooperative agreement by Associated Universities, Inc.

³ Exelis Visual Information Solutions, Boulder, CO.

⁴ <https://www.legacysurvey.org/>

Figure 1. Images of 77 HI-detected nearby late-type dwarf galaxies taken from DESI Legacy Imaging Surveys. Each image side is $2'$, North is to the top and East is to the left.

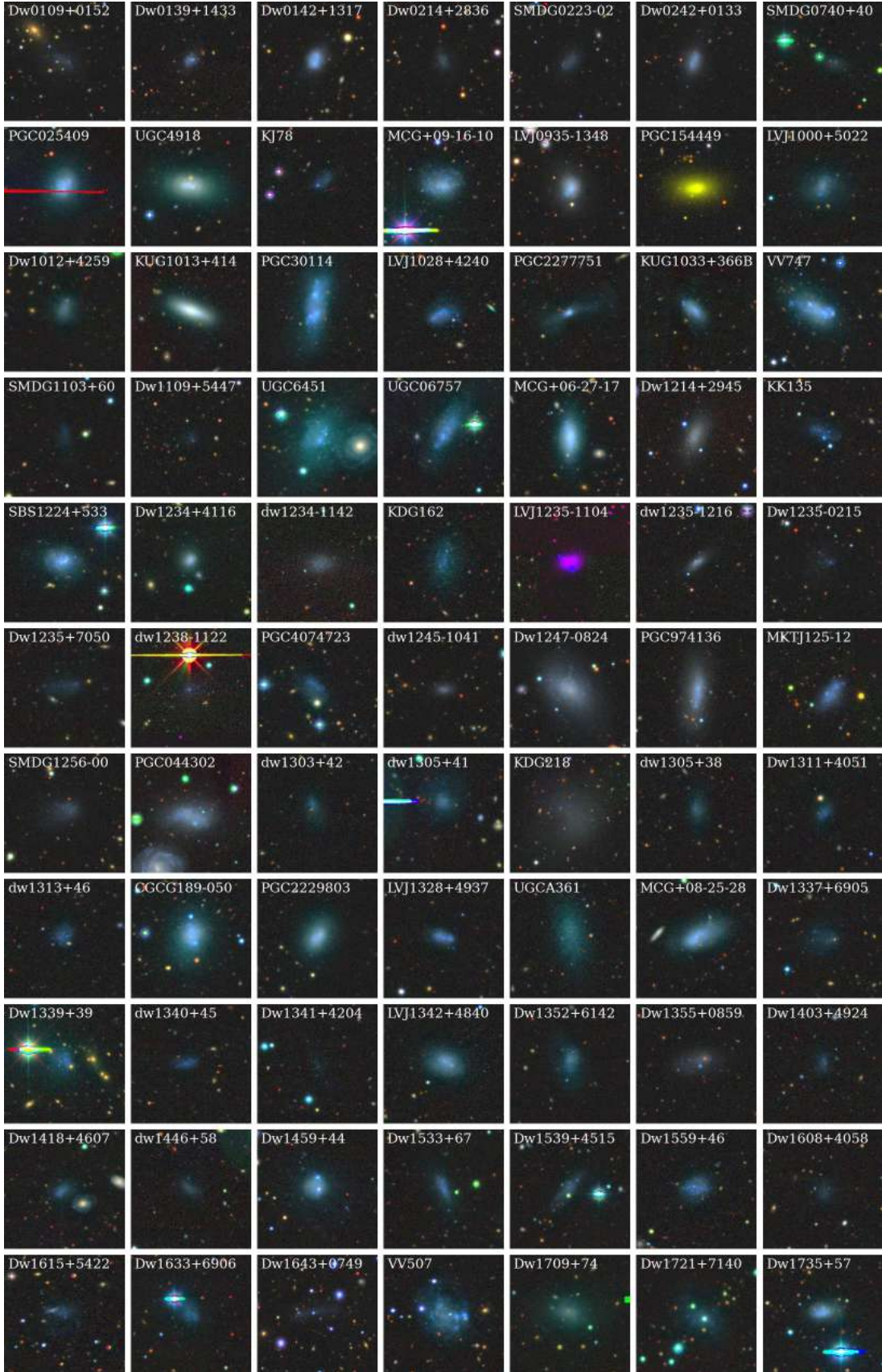


Table 1. List of galaxies detected with GBT.

Bold font indicates that the galaxy is within the LV ($D_{\text{NAM}} < 12$ Mpc).

Name	RA(2000.0)	Dec.	b/a	B mag	$B - V$ mag	V_h km s^{-1}	W_{50} km s^{-1}	S_{HI} Jy km s^{-1}	D_{NAM} Mpc	$\log M_{\text{HI}}$ M_{\odot}	$\log M_*$ M_{\odot}
Dw 0109+0152	01:09:17.0+01:52:59		0.54	18.24	0.61	1163.5 \pm 0.7	24.0 \pm 1.5	0.49 \pm 0.04	15.0	7.41	7.21
Dw 0139+1433	01:39:50.6+14:33:22		0.87	18.25	0.55	757.1 \pm 2.8	26.2 \pm 6.6	0.16 \pm 0.04	10.8	6.64	6.84
Dw 0142+1317	01:42:07.2+13:17:38		0.83	16.72	0.48	804.0 \pm 0.8	43.2 \pm 1.9	1.67 \pm 0.07	11.1	7.69	7.38
Dw 0214+2836	02:14:09.6+28:36:47		0.48	18.98	0.62	2899.1 \pm 2.6	41.5 \pm 6.2	0.26 \pm 0.04	36.1	7.90	7.70
SMDG 0223-02	02:23:18.7-02:03:25		0.67	18.61	0.57	1245.1 \pm 0.9	21.9 \pm 2.2	0.28 \pm 0.03	14.7	7.15	6.99
Dw 0242+0133	02:42:33.1+01:33:50		0.73	17.37	0.60	1195.6 \pm 1.7	23.0 \pm 4.0	0.19 \pm 0.03	14.7	6.98	7.53
SMDG 0740+40	07:40:23.0+40:32:56		0.63	19.18	0.81	353.5 \pm 3.6	38.8 \pm 8.6	0.13 \pm 0.02	10.1	6.49	6.79
PGC 025409	09:02:50.6+71:18:22		0.73	15.79	0.48	408.4 \pm 0.5	38.6 \pm 1.2	1.81 \pm 0.05	10.3	7.65	7.69
UGC 4918	09:19:17.7+69:48:04		0.93	15.73	0.85	723.3 \pm 1.5	32.9 \pm 3.6	0.36 \pm 0.03	14.0	7.22	8.51
KJ78	09:20:36.4+49:40:31		0.62	18.42	0.44	603.8 \pm 0.4	22.0 \pm 0.9	0.89 \pm 0.04	13.2	7.56	6.78
MCG+09-16-10	09:23:17.0+51:58:22		0.78	16.09	0.58	485.5 \pm 0.7	57.5 \pm 1.5	3.09 \pm 0.06	11.0	7.94	7.76
LV J0935-1348	09:35:21.6-13:48:52		0.75	16.44	0.67	811.3 \pm 1.7	50.4 \pm 4.1	0.78 \pm 0.06	11.7	7.40	7.81
PGC 154449	09:57:08.9-09:15:48		0.93	15.98	0.86	562.7 \pm 1.8	36.6 \pm 4.2	0.32 \pm 0.03	8.0	6.68	7.94
LV J1000+5022	10:00:25.5+50:22:45		0.76	16.99	0.66	548.7 \pm 1.2	48.7 \pm 2.8	0.84 \pm 0.05	11.9	7.45	7.58
Dw 1012+4259	10:12:42.7+42:59:31		0.75	17.87	0.72	2297.0 \pm 1.7	49.5 \pm 4.2	0.74 \pm 0.04	37.0	8.37	8.30
KUG 1013+414	10:16:15.6+41:09:58		0.39	15.58	0.77	506.6 \pm 3.2	78.4 \pm 7.5	0.39 \pm 0.03	9.9	6.95	8.14
PGC 30114	10:18:43.0+46:02:44		0.30	15.21	0.42	586.6 \pm 0.6	55.2 \pm 1.3	5.12 \pm 0.07	11.9	8.23	7.94
LV J1028+4240	10:28:33.0+42:40:07		0.71	17.00	0.36	559.0 \pm 0.6	34.2 \pm 1.3	1.83 \pm 0.07	10.6	7.68	7.04
PGC 2277751	10:35:12.1+46:14:12		0.63	17.15	0.60	544.0 \pm 1.9	43.9 \pm 4.5	0.26 \pm 0.03	10.8	6.85	7.35
KUG 1033+366B	10:36:17.6+36:25:31		0.53	17.05	0.58	618.2 \pm 0.9	34.7 \pm 2.1	0.70 \pm 0.04	12.3	7.40	7.47
VV747	10:57:47.0+36:15:39		0.56	15.49	0.46	630.2 \pm 0.7	75.4 \pm 1.6	4.91 \pm 0.08	9.8	8.05	7.73
SMDG 1103+60	11:03:56.4+60:29:53		0.64	19.24	0.46	1060.7 \pm 1.6	27.6 \pm 3.7	0.38 \pm 0.05	18.9	7.51	6.79
Dw 1109+5447	11:09:13.2+54:47:10		0.78	19.80	0.53	724.4 \pm 1.0	27.8 \pm 2.4	0.20 \pm 0.02	13.9	6.95	6.41
UGC 6451	11:28:46.4+79:36:07		0.53	15.44	0.67	49.6 \pm 0.3	28.0 \pm 0.7	2.36 \pm 0.03	3.2	6.75	7.07
UGC 06757	11:46:59.1+61:20:05		0.55	16.09	0.50	88.4 \pm 0.3	25.4 \pm 0.8	1.87 \pm 0.05	2.6	6.48	6.39
MCG+06-27-17	12:09:56.4+36:26:07		0.31	15.52	0.58	326.8 \pm 0.8	49.3 \pm 1.9	1.94 \pm 0.07	4.3	6.93	7.17
Dw 1214+2945	12:14:26.6+29:45:50		0.45	17.27	1.00	457.5 \pm 2.7	33.4 \pm 6.4	0.19 \pm 0.03	5.2	6.07	7.24
KK135	12:19:34.7+58:02:34		0.52	17.74	0.36	142.5 \pm 0.5	20.4 \pm 1.1	0.70 \pm 0.04	2.9	6.14	5.62
SBS 1224+533	12:26:52.6+53:06:19		0.69	16.00	0.46	292.1 \pm 0.5	31.6 \pm 1.2	1.18 \pm 0.04	6.2	7.03	7.12
Dw 1234+4116	12:34:38.2+41:16:34		0.81	17.28	0.76	614.3 \pm 1.4	28.1 \pm 3.4	0.19 \pm 0.03	8.9	6.53	7.36
dw 1234-1142	12:34:48.6-11:42:25		0.84	17.61	0.69	1153.2 \pm 1.6	21.6 \pm 3.9	0.23 \pm 0.04	9.5	6.68	7.19
KDG 162	12:35:01.6+58:23:08		0.69	17.28	0.63	125.3 \pm 0.8	21.8 \pm 1.9	0.53 \pm 0.03	2.9	6.01	6.18
LV J1235-1104	12:35:39.4-11:04:01		0.90	16.86	0.22	1099.7 \pm 0.9	55.4 \pm 2.1	1.97 \pm 0.08	8.8	7.55	6.73
dw 1235-1216	12:35:42.9-12:16:23		0.42	18.21	0.69	1162.1 \pm 1.7	33.3 \pm 3.9	0.33 \pm 0.04	9.7	6.86	6.97
Dw 1235-0215	12:35:53.0-02:15:54		0.82	18.80	0.46	1160.5 \pm 1.3	17.3 \pm 3.0	0.17 \pm 0.04	9.6	6.56	6.38
Dw 1235+7050	12:35:59.5+70:50:53		0.57	18.59	0.67	1844.5 \pm 0.9	28.6 \pm 2.2	0.56 \pm 0.04	30.9	8.10	7.78
dw 1238-1122	12:38:33.6-11:22:05		0.66	18.54	0.73	2319.0 \pm 1.0	24.6 \pm 2.3	0.47 \pm 0.05	33.2	8.08	7.96
PGC 4074723	12:40:29.9+47:22:04		0.70	17.55	0.56	524.4 \pm 0.6	22.4 \pm 1.3	0.69 \pm 0.04	8.4	7.05	6.91
dw 1245-1041	12:45:07.2-10:41:56		0.74	18.84	0.65	1479.4 \pm 1.5	14.6 \pm 3.6	0.08 \pm 0.03	22.3	6.99	7.38
Dw 1247-0824	12:47:25.0-08:24:29		0.66	15.73	0.59	1214.1 \pm 1.3	86.4 \pm 2.7	3.04 \pm 0.10	14.8	8.19	8.18
PGC 974136	12:49:59.5-10:45:22		0.40	16.23	0.65	993.8 \pm 0.9	32.5 \pm 2.2	1.04 \pm 0.05	7.9	7.19	7.52
MKT J125-12	12:52:25.4-12:43:05		0.62	16.89	0.36	1299.8 \pm 0.7	55.5 \pm 1.6	3.06 \pm 0.07	16.8	8.31	7.49
SMDG 1256-00	12:56:35.8-00:31:44		0.67	17.88	0.51	1177.2 \pm 0.8	32.5 \pm 2.0	0.72 \pm 0.04	10.2	7.24	6.87
PGC 044302	12:57:27.7-12:06:28		0.63	15.88	0.55	1407.7 \pm 0.7	44.2 \pm 1.8	1.73 \pm 0.06	18.4	8.14	8.25
dw 1303+42	13:03:14.0+42:22:17		0.63	18.28	0.60	450.2 \pm 2.3	27.0 \pm 5.3	0.22 \pm 0.04	6.4	6.33	6.44

Table 1. continue

Name	RA(2000.0)	Dec.	b/a	B	$B - V$	V_h	W_{50}	S_{HI}	D_{NAM}	$\log M_{HI}$	$\log M_*$
				mag	mag	km s ⁻¹	km s ⁻¹	Jy km s ⁻¹	Mpc	M _⊙	M _⊙
dw 1305+41	13:05:29.0+41:53:24		0.88	17.02	0.41	1154.3±1.3	62.5±3.0	1.55±0.06	21.9	8.24	7.74
KDG 218	13:05:44.0−07:45:20		0.71	16.40	0.65	1474.9±1.6	22.3±3.7	0.28±0.03	22.7	7.52	8.37
dw 1305+38	13:05:58.0+38:05:43		0.70	18.32	0.56	419.6±1.6	28.8±3.6	0.14±0.03	5.3	5.96	6.21
Dw 1311+4051	13:11:41.3+40:51:47		0.61	18.44	0.43	603.0±0.6	24.3±1.5	0.50±0.05	9.3	7.01	6.45
dw 1313+46	13:13:02.0+46:36:08		0.83	17.96	0.34	388.6±0.6	26.6±1.3	0.86±0.04	6.1	6.87	6.14
CGCG 189-050	13:17:04.9+37:57:08		0.77	15.48	0.58	333.6±0.5	30.1±1.1	2.05±0.06	4.2	6.93	7.16
PGC 2229803	13:27:53.1+43:48:55		0.65	16.28	0.66	436.2±0.7	30.5±1.6	0.62±0.05	6.5	6.78	7.33
LV J1328+4937	13:28:31.2+49:37:37		0.55	17.44	0.37	402.3±0.5	26.8±1.1	0.99±0.04	6.6	7.01	6.47
UGC A361	13:32:36.2+49:49:49		0.59	16.76	0.71	216.1±1.6	22.7±3.7	0.11±0.03	3.7	5.57	6.73
MCG+08-25-28	13:36:44.8+44:35:57		0.52	15.99	0.58	485.7±0.7	32.6±1.6	1.00±0.05	7.6	7.13	7.47
Dw 1337+6905	13:37:43.2+69:05:42		0.78	18.09	0.52	1705.0±0.8	39.4±1.9	1.00±0.04	29.2	8.30	7.72
Dw 1339+39	13:39:45.1+39:08:09		0.66	16.99	0.78	674.1±0.5	24.0±1.1	0.80±0.04	9.9	7.26	7.60
dw 1340+45	13:40:37.0+45:41:54		0.42	18.44	0.37	1385.8±1.0	30.7±2.3	0.70±0.04	25.0	8.01	7.23
Dw 1341+4204	13:41:58.8+42:04:05		0.77	19.45	0.45	248.6±0.9	17.1±2.0	0.16±0.02	3.7	5.70	5.27
LV J1342+4840	13:42:20.1+48:40:57		0.69	16.52	0.58	438.3±0.8	25.2±1.8	0.52±0.04	7.4	6.82	7.23
Dw 1352+6142	13:52:39.4+61:42:50		0.56	17.44	0.58	2111.4±1.6	67.1±4.0	1.35±0.06	34.2	8.57	8.20
Dw 1355+0859	13:55:58.7+08:59:39		0.48	17.78	0.81	1219.6±3.0	44.7±7.0	0.38±0.05	18.2	7.47	7.85
Dw 1403+4924	14:03:19.0+49:24:54		0.72	18.94	0.54	2033.0±1.3	23.5±3.1	0.29±0.04	32.2	7.85	7.50
Dw 1418+4607	14:18:31.5+46:07:51		0.63	18.21	0.60	1825.3±1.4	26.5±3.3	0.42±0.04	28.6	7.91	7.76
dw 1446+58	14:46:01.0+58:34:05		0.65	18.80	0.59	2300.3±2.8	47.1±6.6	0.51±0.05	36.8	8.21	7.73
Dw 1459+44	14:59:38.4+44:40:23		0.95	16.09	0.47	732.4±1.1	80.1±2.3	5.16±0.15	14.5	8.40	7.84
Dw 1533+67	15:33:28.1+67:45:29		0.32	17.57	0.54	397.6±0.6	21.4±1.4	0.41±0.04	10.1	6.99	7.04
Dw 1539+4515	15:39:25.9+45:15:04		0.34	17.97	0.61	2605.6±2.5	60.6±5.9	0.66±0.05	40.3	8.40	8.17
Dw 1559+46	15:59:02.6+46:23:40		0.88	17.10	0.43	76.7±0.4	28.5±1.0	1.42±0.04	3.3	6.56	6.09
Dw 1608+4058	16:08:19.4+40:58:12		0.87	18.89	0.39	1982.1±1.0	28.5±2.5	0.48±0.04	30.9	8.03	7.25
Dw 1615+5422	16:15:42.1+54:22:03		0.82	18.09	0.38	3697.3±0.7	52.2±1.6	1.81±0.06	57.1	9.14	8.10
Dw 1633+6906	16:33:01.4+69:06:04		0.85	18.00	0.59	1122.9±1.1	35.8±2.5	0.85±0.05	19.6	7.88	7.50
Dw 1643+0749	16:43:25.1+07:49:30		0.30	18.84	0.51	1434.6±1.5	18.4±3.5	0.19±0.03	19.6	7.23	7.07
VV 507	17:00:42.2+53:21:36		0.81	16.00	0.41	1122.6±0.3	46.0±0.7	3.39±0.05	20.0	8.50	8.07
Dw 1709+74	17:09:45.6+74:10:44		0.81	17.17	0.97	1325.4±2.9	48.3±7.0	0.41±0.05	21.8	7.65	8.48
Dw 1721+7140	17:21:45.4+71:40:59		0.68	17.25	0.60	1076.1±0.6	36.2±1.4	1.58±0.05	18.6	8.11	7.77
Dw 1735+57	17:35:34.6+57:48:47		0.61	16.75	0.53	42.9±0.4	25.7±1.0	0.90±0.03	4.4	6.61	6.64

The remaining 28 undetected galaxies are presented in Table 2, where the column designations are the same as for the first five columns of Table 1. Their Legacy Survey images are shown in Fig. 3 (except KKR56, which is from from Pan-STARRS1). The size $2' \times 2'$ and orientation (North up and East to the left) are the same as in Fig. 1.

It should be noted that the majority of our targets belong to the late morphological types: irregular (Irr), Magellanic (Im), blue compact dwarf (BCD), rich in neutral hydrogen. Some dwarf galaxies are classified as Tr-type, a transitional type between irregular and spheroidal (dSph) dwarfs. Along with dwarf galaxies of the late types, we included in the target

list only one nearby dSph object, Dw 0910+7326, in order to check the presence of neutral hydrogen in it. According to subsequent optical spectral observations (Karachentsev et al. 2025), five of the undetected galaxies, Dw 1234+76, Dw 1245+6158, Dw 1558+67, Dw 1645+46 and SMDG 0956+82, are low-velocity objects, whose HI line is confused with local Galactic hydrogen.

Table 3 contains a summary of our GBT targets that have independent radial velocity measurements obtained with the 500-m FAST radio telescope (Zhang et al. 2024; Karachentsev et al. 2024b) as well as with optical measurements collected in the current version of the UNGC catalog (Karachentsev et al. 2013). Our mea-

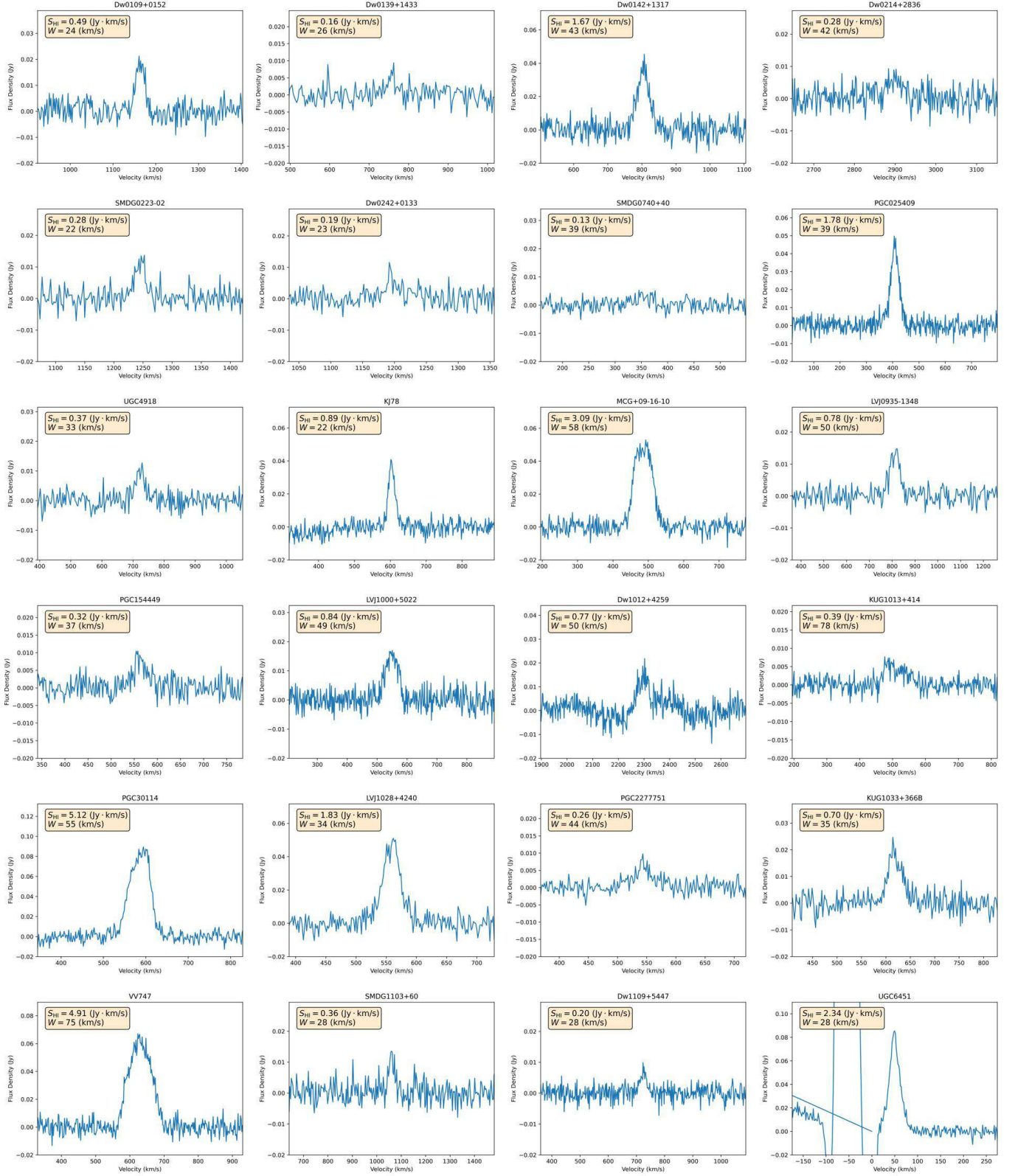
Figure 2. HI spectra of 77 dwarf galaxies detected with GBT. The HI flux integrals and W_{50} values are given above each panel.

Figure 2. Continue

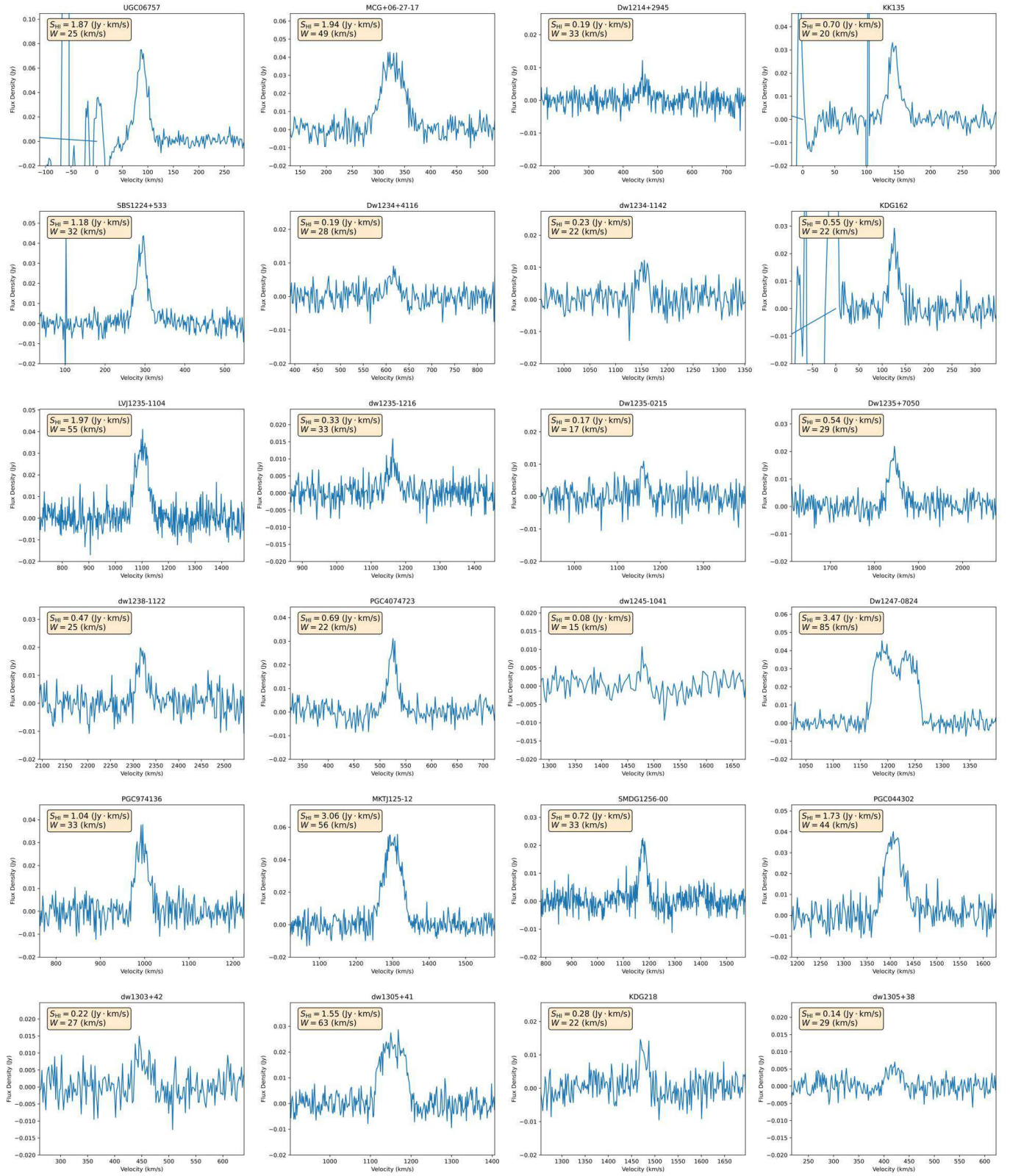


Table 2. List of galaxies not detected with GBT.

Name	RA(2000.0)	Dec	b/a	B mag	$B - V$ mag
[KKS2000] 05	02:49:26.1	-13:12:42	0.43	17.62	0.59
NGC 2337dw1	07:08:29.7	+44:37:26	0.77	18.75	0.77
Dw 0910+7326	09:10:15.6	+73:26:24	0.88	17.40	1.29
Dw 0916+6944	09:16:43.7	+69:44:01	0.33	19.75	0.71
Dw 0927+6818	09:27:27.8	+68:18:55	0.76	19.43	0.88
SMDG 0956+82	09:56:13.0	+82:53:24	0.60	17.99	0.67
Dw 1037+09	10:37:40.6	+09:06:20	0.77	18.90	0.82
[KK98] 108	11:40:03.6	+46:28:43	0.84	17.70	0.77
Dw 1155+78	11:55:54.2	+78:04:44	0.73	19.17	0.65
[KK98] 125	12:12:41.9	+68:55:38	0.87	17.40	
KKH78	12:17:44.5	+33:20:43	0.63	18.29	0.73
Dw 1224+8116	12:24:49.7	+81:16:59	0.44	19.36	0.83
Dw 1234+76	12:34:23.3	+76:43:34	0.58	17.97	0.75
Dw 1238+3337	12:38:18.0	+33:37:59	0.92	17.66	0.67
SMDG 1241+35	12:41:11.0	+35:11:46	0.92	18.73	0.75
Dw 1245+6158	12:45:49.0	+61:58:08	0.49	18.42	0.72
Dw 1252-0904	12:52:03.4	-09:04:26	0.70	19.62	0.35
Dw 1259-1735	12:59:40.3	-17:35:46	0.53	18.11	0.63
KK 207	13:33:25.7	+56:30:00	0.70	18.38	0.48
SMDG 1345+33	13:45:11.0	+33:11:31	0.86	19.23	0.73
Dw 1349+5943	13:49:50.9	+59:43:44	0.90	20.13	0.85
Dw 1351+5014	13:51:59.0	+50:14:53	0.82	20.50	
Dw 1354+4446	13:54:10.1	+44:46:48	0.80		
Dw 1441+5136	14:41:56.6	+51:36:40	0.57	19.56	0.69
Dw 1558+67	15:58:46.8	+67:51:29	0.87	16.75	0.47
Dw 1617+4609	16:17:35.8	+46:09:32	0.48	19.28	0.47
Dw 1645+46	16:45:48.5	+46:47:24	0.67	17.61	0.52
KKR56	20:48:24.1	+58:37:06	0.64	17.60	

The upper limit of the flux for the undetected sources is about $0.09 \text{ Jy km s}^{-1}$, which corresponds to $m_{21} = 20^{\text{m}0}$.

measurements are in excellent agreement with the FASHI survey in terms of velocity: $\langle V^{\text{FAST}} - V^{\text{GBT}} \rangle = -0.4 \pm 0.7 \text{ km s}^{-1}$ with standard deviation of $\sigma_V = 3.7 \text{ km s}^{-1}$; HI line width at the 50% level: $\langle W_{50}^{\text{FAST}} - W_{50}^{\text{GBT}} \rangle = 0.9 \pm 0.8 \text{ km s}^{-1}$ and $\sigma_{W_{50}} = 4.3 \text{ km s}^{-1}$; and total flux: $\langle S_{\text{HI}}^{\text{FAST}} - S_{\text{HI}}^{\text{GBT}} \rangle = -0.09 \pm 0.06 \text{ Jy km s}^{-1}$ and $\sigma_S = 0.33 \text{ Jy km s}^{-1}$. Comparison of the GBT measurements with data collected in the LV database gives $\langle V^{\text{UNGC}} - V^{\text{GBT}} \rangle = -19 \pm 10 \text{ km s}^{-1}$ with $\sigma = 59 \text{ km s}^{-1}$, which turns out to be noticeably worse due to the low accuracy of optical velocity measurements.

4. NOTES ON INDIVIDUAL OBJECTS

Dw 0139+1433. According to [Carlsten et al. \(2022\)](#), its distance is $D = 10.82 \text{ Mpc}$. This dwarf is a probable satellite of the spiral galaxy NGC 628 or NGC 660.

Dw 0142+1317. A probable companion to the ring-like spiral galaxy NGC 660.

Dw 0214+2836. Sb galaxy NGC 865 with a radial velocity of $V_h = 2995 \text{ km s}^{-1}$ is located $27'$ South.

SMDG 0223-02. A probable satellite of UGC 1862.

[KKS 2000]05. Isolated irregular dwarf with smooth structure and a knot on the NW side.

SMDG 0740+40. It is probably associated with a brighter dwarf, DDO 46, having the distance $D = 10.4 \text{ Mpc}$ via TRGB.

PGC 025409. Isolated dIrr galaxy with granular structure at the center.

Dw 0910+7326. A new spheroidal dwarf near the M 81 group discovered by [Karachentsev & Kaisina \(2022\)](#) with a distance of 3.21 Mpc ([Casey et al. 2023](#)).

Dw 0916+6944. Isolated dIrr with granular structure or a distant spiral galaxy of low surface brightness.

UGC 4918. A satellite of SB0 galaxy NGC 2787 that has a radial velocity of $V_h = 700 \text{ km s}^{-1}$.

Dw 0927+6818. An object of low surface brightness, a probable satellite of NGC 2787.

Dw 1012+4259. A probable satellite of S0a galaxy IC 598 that has $V_h = 2245 \text{ km s}^{-1}$.

Dw 1109+5447. A new dIrr satellite of Scd galaxy NGC 3556 that has $V_h = 696 \text{ km s}^{-1}$ and TF-distance of 9.9 Mpc (UNGC).

UGC 6451. A new remote member of the M 81 group, being in contact with a distant spiral galaxy UGC 6450.

Dw 1214+2945. A dwarf galaxy of smooth structure located in the region of Coma-I group, which is characterized with a high negative peculiar velocity ([Abazajian et al. 2009](#)).

Dw 1234+76. An isolated dwarf with granular structure and an optical velocity $V_h = 202 \pm 76 \text{ km s}^{-1}$ ([Karachentsev et al. 2025](#)).

Dw 1234+4116. A blue compact dwarf, a satellite of the interacting galaxy pair NGC 4490/85.

dw 1234-1142, LV J1235-1104, dw 1235-1216, PGC 974136. These are likely members of the galaxy group around NGC 4594 (Sombrero).

KDG 162. A blue semi-resolved dwarf, probably associated with Sm-galaxy NGC 4605 that has $V_h = 151 \text{ km s}^{-1}$ and TRGB-distance of 5.55 Mpc (UNGC).

Dw 1235-0215. dIrr galaxy with an asymmetric shape and granular structure as seen in Hyper Suprime-Cam (HSC) archive of the Subaru telescope. It is probably associated with NGC 4594 (Sombrero) that has $V_h = 1090 \text{ km s}^{-1}$ and TRGB-distance of 9.55 Mpc .

Dw 1238+3337. An isolated blue dwarf with smoothed structure. Its optical velocity is $V_h = 1083 \pm 10 \text{ km s}^{-1}$ ([Karachentsev et al. 2025](#)).

Table 3. Comparison of radial velocity and HI measurements.

Name	RA(2000.0) Dec	GBT			FASHI			UNGC
		V_h km s ⁻¹	S_{HI} Jy km s ⁻¹	W_{50} km s ⁻¹	V_h km s ⁻¹	S_{HI} Jy km s ⁻¹	W_{50} km s ⁻¹	V_h km s ⁻¹
PGC 025409	09:02:50.6+71:18:22	408.4±0.5						416±10
UGC 4918	09:19:17.7+69:48:04	723.3±1.5						710±41
KJ78	09:20:36.4+49:40:31	603.8±0.4	0.89±0.04	22.0±0.9	606.1±0.6	0.74±0.06	22.4±1.2	477±30
MCG+09-16-10	09:23:17.0+51:58:22	485.5±0.7	3.09±0.06	57.5±1.5	485.5±0.5	3.80±0.13	65.8±1.0	484±4
LV J0935-1348	09:35:21.6-13:48:52	811.3±1.7						796±45
PGC 154449	09:57:08.9-09:15:48	562.7±1.8						543±45
LV J1000+5022	10:00:25.5+50:22:45	548.7±1.2	0.84±0.05	48.7±2.8	551.1±1.2	0.73±0.08	52.6±2.4	538±11
Dw 1012+4259	10:12:42.7+42:59:31	2297.0±1.7	0.74±0.04	49.5±4.2	2296.0±1.8	0.53±0.08	52.9±3.5	2326±47
KUG 1013+414	10:16:15.6+41:09:58	506.6±3.2						518±1
PGC 30114	10:18:43.0+46:02:44	586.6±0.6	5.12±0.07	55.2±1.3	584.5±0.2	5.61±0.10	59.5±0.4	566±256
LV J1028+4240	10:28:33.0+42:40:07	559.0±0.6	1.83±0.07	34.2±1.3	557.2±0.4	1.70±0.07	30.2±0.8	547±5
PGC 2277751	10:35:12.1+46:14:12	544.0±1.9						505±23
KUG 1033+366B	10:36:17.6+36:25:31	618.2±0.9	0.70±0.04	34.7±2.1	619.1±0.7	0.75±0.07	32.2±1.5	620±2
VV747	10:57:47.0+36:15:39	630.2±0.7	4.91±0.08	75.4±1.6	628.3±0.4	5.92±0.15	84.8±0.8	619±2
SMDG 1103+60	11:03:56.4+60:29:53	1060.7±1.6	0.38±0.05	27.6±3.7	1059.9±1.2	0.33±0.06	30.4±2.3	
UGC 6451	11:28:46.4+79:36:07	49.6±0.3						33±20
UGC 06757	11:46:59.1+61:20:05	88.4±0.3						82±4
MCG+06-27-17	12:09:56.4+36:26:07	326.8±0.8	1.94±0.07	49.3±1.9	325.5±1.2	1.56±0.14	47.6±2.4	
Dw 1214+2945	12:14:26.6+29:45:50	457.5±2.7						426±69
KK135	12:19:34.7+58:02:34	142.5±0.5						215±40
SBS1224+533	12:26:52.6+53:06:19	292.1±0.5	1.18±0.04	31.6±1.2	291.4±0.5	1.50±0.08	31.0±0.9	300±3
Dw 1234+4116	12:34:38.2+41:16:34	614.3±1.4						601±3
KDG 162	12:35:01.6+58:23:08	125.3±0.8						105±50
LV J1235-1104	12:35:39.4-11:04:01	1099.7±0.9						1110±10
PGC 4074723	12:40:29.9+47:22:04	524.4±0.6	0.69±0.04	22.4±1.3	522.8±0.6	0.55±0.04	20.1±1.2	229±132
Dw 1247-0824	12:47:25.0-08:24:29	524.4±0.6						1215±10
dw 1303+42	13:03:14.0+42:22:17	450.2±2.3	0.22±0.04	27.0±5.3	448.9±0.9	0.33±0.03	32.7±1.9	
Dw 1311+4051	13:11:41.3+40:51:47	603.0±0.6	0.50±0.05	24.3±1.5	604.2±0.8	0.52±0.07	21.3±1.7	
dw 1313+46	13:13:02.0+46:36:08	388.6±0.6	0.86±0.04	26.6±1.3	388.5±0.5	0.95±0.06	26.9±1.1	
CGCG 189-050	13:17:04.9+37:57:08	333.6±0.5	2.05±0.06	30.1±1.1	333.5±0.4	2.27±0.07	27.1±0.7	324±6
PGC 2229803	13:27:53.1+43:48:55	436.2±0.7	0.62±0.05	30.5±1.6	433.9±0.8	0.64±0.07	29.9±1.7	452±39
LV J1328+4937	13:28:31.2+49:37:37	402.3±0.5	0.99±0.04	26.8±1.1	400.8±0.6	0.96±0.07	21.7±1.2	395±9
MCG+08-25-28	13:36:44.8+44:35:57	485.7±0.7	1.00±0.05	32.6±1.6	487.9±0.8	1.04±0.08	30.3±1.5	
Dw 1339+39	13:39:45.1+39:08:09	674.1±0.5	0.80±0.04	24.0±1.1	681.9±0.7	1.03±0.07	25.4±1.4	
dw 1340+45	13:40:37.0+45:41:54	1385.8±1.0	0.70±0.04	30.7±2.3	1375.9±1.8	0.79±0.11	36.3±3.5	
LV J1342+4840	13:42:20.1+48:40:57	438.3±0.8	0.52±0.04	25.2±1.8	434.5±0.8	0.60±0.05	22.5±1.6	438±2
Dw 1352+6142	13:52:39.4+61:42:50	2111.4±1.6	1.35±0.06	67.1±4.0	2111.2±0.9	1.75±0.11	66.2±1.7	
Dw 1403+4924	14:03:19.0+49:24:54	2033.0±1.3	0.29±0.04	23.5±3.1	2022.5±1.7	0.38±0.06	28.0±3.3	
Dw 1418+4607	14:18:31.5+46:07:51	1825.3±1.4	0.42±0.04	26.5±3.3	1829.5±1.1	0.43±0.07	32.1±2.1	
dw 1446+58	14:46:01.0+58:34:05	2300.3±2.8	0.51±0.05	47.1±6.6	2299.4±1.1	0.41±0.05	40.9±2.3	
Dw 1459+44	14:59:38.4+44:40:23	732.4±1.1	5.16±0.15	80.1±2.3	732.8±0.2	5.86±0.11	80.8±0.5	683±15
Dw 1539+4515	15:39:25.9+45:15:04	2605.6±2.5	0.66±0.05	60.6±5.9	2607.5±1.4	0.53±0.07	69.5±2.9	
Dw 1559+46	15:59:02.6+46:23:40	76.7±0.4						67±10
Dw 1615+5422	16:15:42.1+54:22:03	3697.3±0.7	1.81±0.06	52.2±1.6	3703.8±0.3	1.18±0.03	47.3±0.6	
Dw 1709+74	17:09:45.6+74:10:44	1325.4±2.9						1298±10
Dw 1735+57	17:35:34.6+57:48:47	42.9±0.4						42±10

Figure 2. Continue

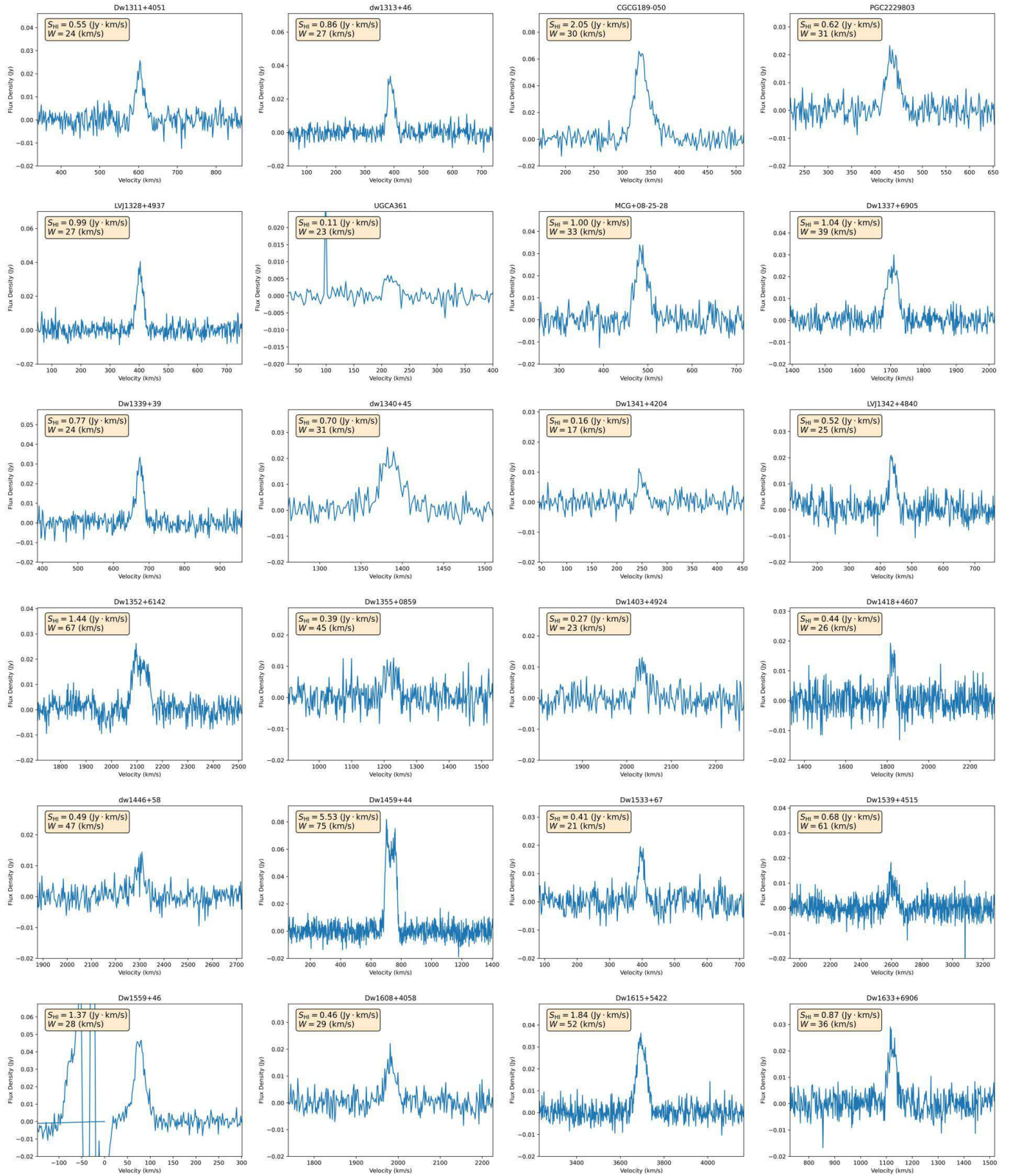


Figure 2. Continue

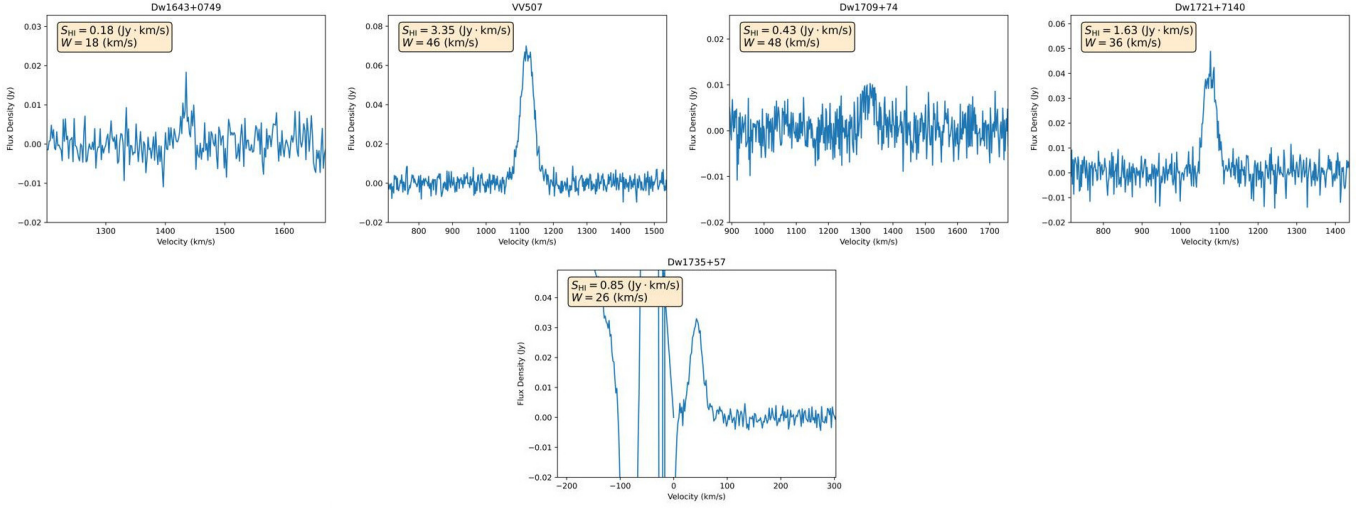
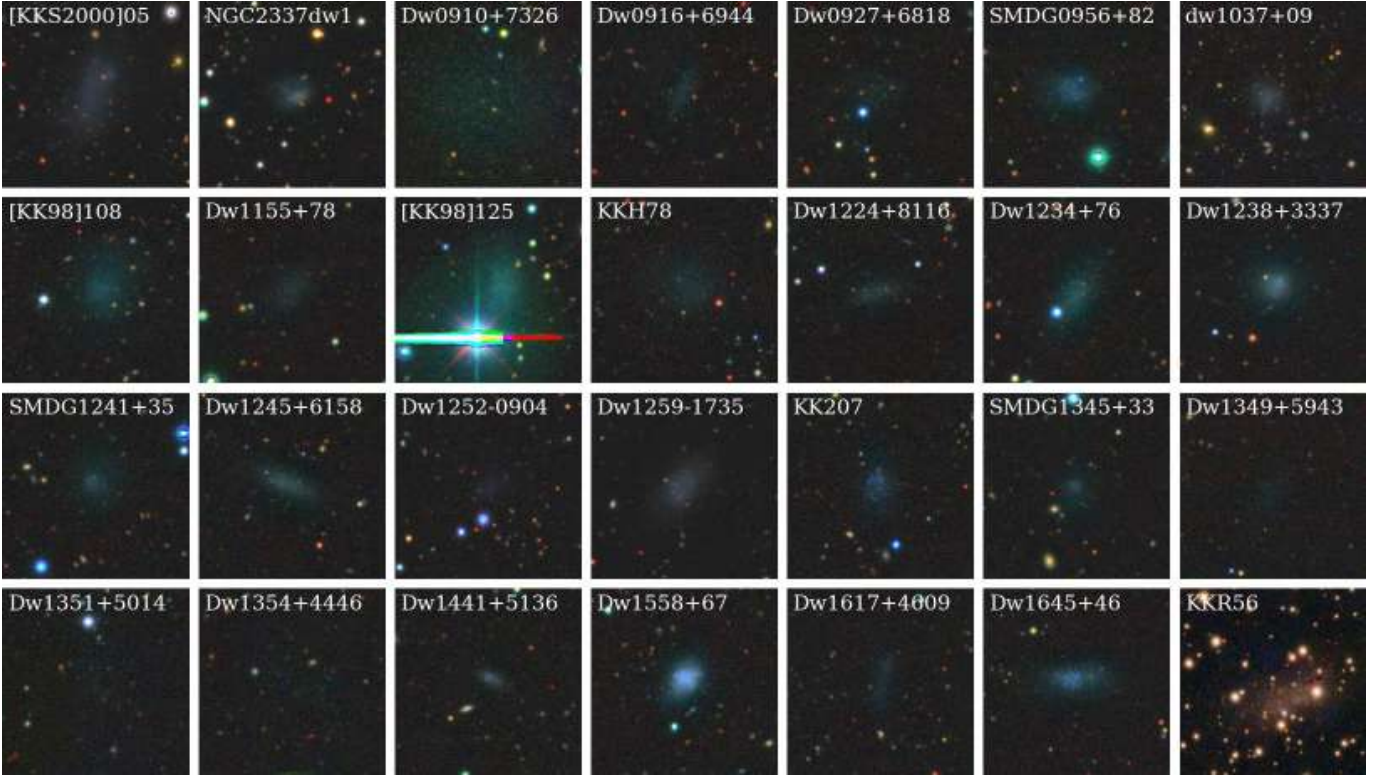


Figure 3. Images of 28 undetected nearby late-type dwarf galaxies taken from DESI Legacy Imaging Surveys (*KKR56* from PanSTARRS). Each image side is $2'$, North is to the top and East is to the left.



SMDG 1241+35. Its optical velocity is $V_h = 661 \pm 10$ km s $^{-1}$ (Karachentsev et al. 2025). A probable satellite of NGC 4631.

Dw 1245+6158. Its optical velocity is $V_h = 68 \pm 10$ km s $^{-1}$ (Karachentsev et al. 2025). A probable satellite of NGC 4605.

Dw 1247-0824. A blue compact dwarf. Based on its double-horned HI-line, it is more likely a member of the Virgo Southern Extension than a companion to the Sombrero galaxy.

SMDG 1256-00. A possible peripheral member of the Virgo cluster.

KDG 218. An Ultra-Diffuse Dwarf galaxy at a distance of 12.59 Mpc via TRGB (Karachentsev et al. 2018).

Dw 1305+38. A probable peripheral companion to the spiral galaxy NGC 5055.

Dw 1311+4051. A new satellite of the galaxy M63 = NGC 5055 that has $V_h = 500 \text{ km s}^{-1}$ and TRGB-distance of 9.04 Mpc.

UGCA 361. Based on its low radial velocity (216 km s^{-1}) and corresponding kinematic distance of 4.0 Mpc, this is an isolated dwarf located in front of the M51 group and classified as Tr type.

KK 207. An irregular dwarf with granular structure.

Dw 1339+39. An isolated irregular dwarf. At a separation of $46'$ to NE from it, there is another dIrr galaxy DDO 182 with $V_h = 663 \text{ km s}^{-1}$.

Dw 1341+4204. Possibly a new peripheral member of the M101/M63/M51 filament. It is of a very low surface brightness (see HSC archive) and HI-rich.

Dw 1351+5014. Karachentseva et al. (2023) discovered it as ‘a dwarf galaxy [...] of very low surface brightness, which is barely visible in the SDSS survey’. However, deep g -band images from the Hyper Suprime-Cam Legacy Archive (Tanaka et al. 2021) revealed the absence of a real dwarf galaxy there.

Dw 1352+6142. A probable member of a group around the spiral galaxy UGC 8822.

Dw 1354+4446. It was found in the images of the DESI Legacy Surveys as a very low surface brightness object, however more deep images of the Hyper Suprime-Cam Subaru Strategic Program DR2 (Aihara et al. 2019) show no real nearby dwarf galaxy there.

Dw 1403+4924. It is $16'$ away from Sa galaxy NGC 5448 that has $V_h = 2016 \text{ km s}^{-1}$.

Dw 1418+4607. Isolated blue compact dwarf projected into a distant pair of galaxies.

dw 1446+58. A probable member of a scattered group of galaxies around Sb galaxy NGC 5777 that has $V_h = 2139 \text{ km s}^{-1}$.

Dw 1459+44. A blue compact dwarf with a large faint halo (see the HSC archive). At a projected separation of $16'$ from it to the East, there is another BCD galaxy UGC 9660 with $V_h = 608 \text{ km s}^{-1}$ and TRGB-distance of 10.76 Mpc (UNGC).

Dw 1533+67. An isolated dIrr. At a projected separation of $55'$ to SE from it, there is another dIrr galaxy UGC 9992 with $V_h = 423 \text{ km s}^{-1}$ and TRGB-distance of 11.27 Mpc (UNGC).

Dw 1539+4515. An isolated dIrr with patchy structure.

Dw 1558+67. An isolated blue compact dwarf with granular structure and the optical velocity of $V_h =$

$-25 \pm 10 \text{ km s}^{-1}$ (Karachentsev et al. 2025). The lack of HI emission may be caused by confusion of the HI-line from the galaxy with the local Milky Way emission.

Dw 1559+46. An isolated blue compact dwarf with granular structure.

Dw 1608+4058. An isolated dIrr with smooth structure. Possibly associated with a group around Sab galaxy UGC 10200 = Mrk 1104 having $V_h = 1991 \text{ km s}^{-1}$.

Dw 1615+5422. A peculiar spiral or an interacting binary system. Bright in the FUV -band.

Dw 1617+4609. An isolated dIrr galaxy of low surface brightness.

Dw 1645+46. An isolated dIrr galaxy semi-resolved into stars, with the optical velocity of $V_h = -21 \pm 10 \text{ km s}^{-1}$ (Karachentsev et al. 2025). Its HI-line is masked by the hydrogen emission from our Galaxy.

VV 507 = I Zw 171. Peculiar blue patchy galaxy. Surprisingly, this bright object still had no measured radial velocity. At $59'$ to the West from it, there is a dwarf Sm galaxy DDO 206 = UGC 10608 with $V_h = 1090 \text{ km s}^{-1}$.

Dw 1735+57. An isolated blue compact dwarf with granular structure and a negative optical velocity.

5. DISCUSSION

The sample of 77 HI-detected galaxies is characterized by the following median values: radial velocity of $V_h = 732 \text{ km s}^{-1}$, HI line width of 32 km s^{-1} , HI-flux of $0.70 \text{ Jy km s}^{-1}$, and kinematic NAM distance of 11.0 Mpc. According to the NAM, 43 galaxies fall into the Local Volume with $D_{\text{NAM}} < 12 \text{ Mpc}$. The average color of the 77 detected dwarf galaxies is

$$\langle B - V \rangle = 0.57 \pm 0.02 \text{ mag.} \quad (1)$$

while the 24 (out of 28) undetected ones have color of

$$\langle B - V \rangle = 0.70 \pm 0.04 \text{ mag.} \quad (2)$$

Following Giovanelli et al. (2005), we determined the hydrogen mass of the galaxy as

$$M_{\text{HI}}/M_{\odot} = 2.36 \times 10^5 D_{\text{Mpc}}^2 S_{\text{HI}}, \quad (3)$$

which gives

$$\log(M_{\text{HI}}/M_{\odot}) = 12.33 + 2 \log D_{\text{Mpc}} - 0.4 m_{21}, \quad (4)$$

where the mass is expressed in mass of the Sun and

$$m_{21} = 17.4 - 2.5 \log(S_{\text{HI}}) \quad (5)$$

according to the formula adopted in the Third Reference Catalogue of Bright Galaxies (RC3, de Vaucouleurs et al. 1991) and in the HyperLEDA database (Makarov

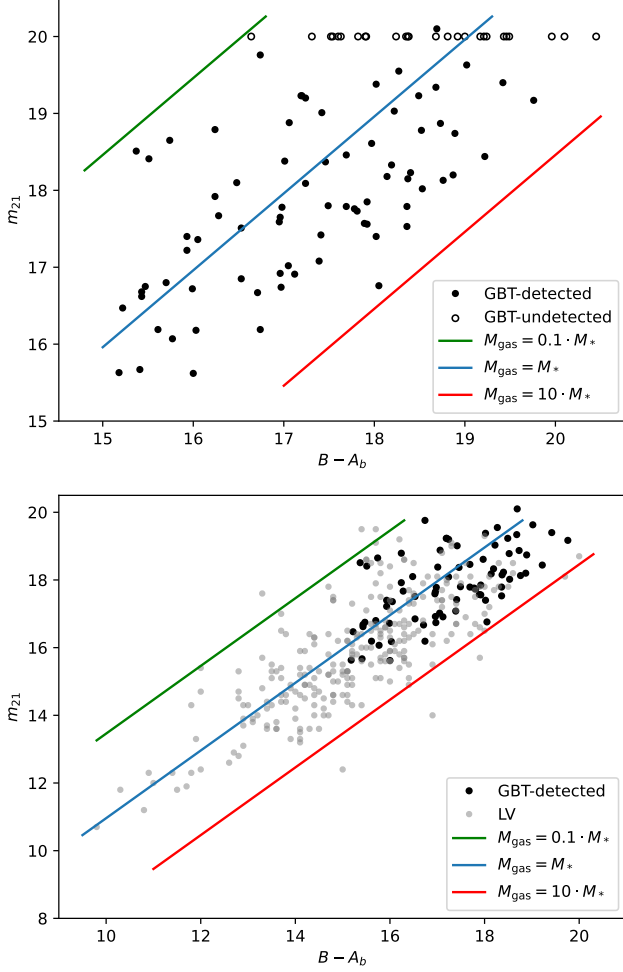


Figure 4. *Upper panel.* Distribution of 105 observed dwarf galaxies according to m_{21} magnitude and B -magnitude corrected for Galactic extinction. Three diagonal lines indicate a ratio $\mu = M_{\text{gas}}/M_*$ equal to 0.1, 1, and 10. For undetected galaxies the $m_{21} = 20^m0$ is assigned. *Bottom panel.* Distribution of 77 GBT-detected dwarf galaxies according to m_{21} magnitude and B -magnitude corrected for Galactic extinction combined with 266 late-type ($T = 9, 10$) dwarf galaxies in the Local Volume with TRGB distance estimates. Three diagonal lines correspond to μ equal to 0.1, 1, and 10.

et al. 2014). Taking heavy elements into account, the mass of neutral gas in a galaxy is usually represented as

$$M_{\text{gas}} = 1.4M_{\text{HI}}. \quad (6)$$

To estimate the stellar mass, we use the M/L relation

$$\log(M_*/L_B) = -0.91 + 1.45(B - V), \quad (7)$$

justified by Herrmann et al. (2016), where B and V magnitudes are corrected for the Galactic extinction, and the B -band luminosity is related to the absolute B -magnitude, M_B , in the standard way

$$\log(L_B/L_\odot) = 0.4(M_{B,\odot} - M_B). \quad (8)$$

Using $M_{B,\odot} = 5.44$ (Willmer 2018), the stellar mass of a galaxy can be expressed as

$$\log(M_*/M_\odot) = 11.27 + 2\log(D_{\text{Mpc}}) + 1.45(B - V) - 0.4B. \quad (9)$$

As a result, the equality $M_{\text{gas}} = M_*$ occurs when

$$m_{21} = B + 0.96 \pm 0.07 \text{ mag}. \quad (10)$$

Consequently, in the late-type dwarf galaxies with $m_{21} - B < 0^m96$, the gas component dominates.

According to Sardone et al. (2021), deep observations with the GBT down to a column density of $N_{\text{HI}} = 6 \times 10^{17} \text{ cm}^{-2}$ over a 20 km s^{-1} line-width reveal that a fraction of diffuse neutral gas below the $N_{\text{HI}} < 10^{19} \text{ cm}^{-2}$ level ranges from 5 to 93% of the total HI mass. The typical rms noise in our observations is 3.3 mJy, which is at least no worse than the noise level of 3.2–10.4 mJy in the Sardone et al. (2021) cubes. Therefore, we can be confident that the total gas masses measured in our survey also include a diffuse component outside the main HI-disk of dwarf galaxies.

The distribution of galaxies in our sample according to m_{21} and B magnitudes is presented in the top panel of Fig. 4. Galaxies undetected in the HI line are shown as open circles with $m_{21} = 20.0$, which corresponds to the upper limit of the flux for these sources of about $0.09 \text{ Jy km s}^{-1}$. The diagonal lines on Fig. 4 correspond to $\mu = M_{\text{gas}}/M_*$ equal to 0.1, 1.0 and 10. As can be seen from these data, most detected galaxies are gas-dominated systems with the median gas-to-star mass ratio $\mu = 1.87$.

The hydrogen mass of the detected galaxies lies in the interval $\log(M_{\text{HI}}/M_\odot) = [5.57 - 9.14]$ with the median of 7.24. Based on the distribution of undetected galaxies at the upper edge of the diagram, their median μ value does not exceed 1. Mostly transition-type galaxies (Tr) fall into this category. Note that kinematic distances D_{NAM} were used to estimate the galaxy masses.

The current version of the UNGC catalog contains 275 dwarf galaxies of the late types ($T = 9$ and 10) with accurate TRGB distance estimates. We excluded from consideration three galaxies of the M81 group (BK3N, HS117, DDO82) where the HI line is masked by the local Galactic hydrogen emission, and six galaxies in the Zone of Avoidance with $A_B > 2^m0$. The distribution of 266 remaining galaxies by m_{21} and $B - A_B$ magnitudes is presented in the bottom panel of Fig. 4. It demonstrates that 97% of late-type dwarfs reside in the range $\mu = [0.1 - 10]$ with the median of about $\mu = 1.5$. The most gas-rich dIrr galaxies (AndIV and ESO215-009) have $\mu = 32$ and 26, respectively. The galaxies we detected (upper panel in Fig. 4) tend to be located in the upper right corner on the bottom panel.

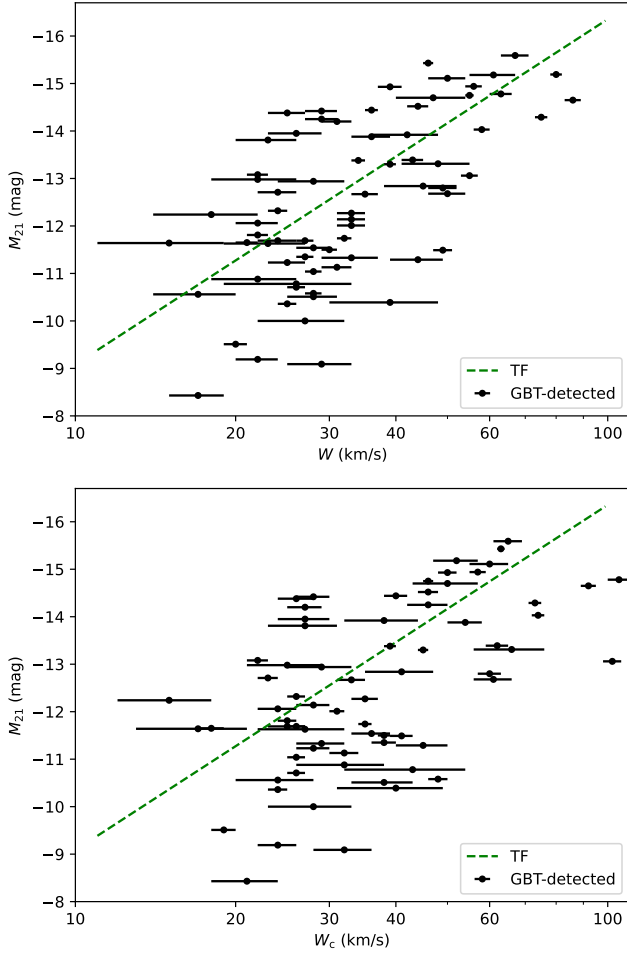


Figure 5. *Upper panel.* Magnitude vs. line width relation for nearby dwarf galaxies detected with the GBT. The horizontal bars indicate the standard errors of W_{50} . The dashed line displays the Tully-Fisher relation, eq.(10). *Bottom panel.* Magnitude vs. line width relation for the same galaxies but with a correction for galaxy inclination according to eq.(13).

Being mainly gas-dominated systems, late-type dwarfs show the expected correlation between their hydrogen mass and HI line width W_{50} , which is the gaseous analogue of the Tully-Fisher relation (Tully & Fisher 1977) between the integral absolute magnitude of galaxy, M_B , and W_{50} . The upper panel of Fig. 5 displays the relation between $M_{21} = m_{21} - 5 \log(D_{\text{Mpc}}) - 25$ and W_{50} for 71 detected galaxies.⁵

Here we excluded the galaxy Dw 1615+5422 (a peculiar spiral system) and five reddish galaxies (UGC 4918, PGC 154449, KUG 1013+414, Dw 1214+2945, and

UGCA 361) that have a smooth structure and low gas content ($M_{\text{gas}}/M_* < 0.1$). The horizontal bars indicate the standard errors of W_{50} given in Table 1. The dashed line in the panel indicates the relation

$$M_B = -7.27(\log W_{50} - 2.5) - 19.99 \quad (11)$$

according to Tully et al. (2008) that has been obtained for luminous disc-dominated galaxies. As follows from these data, dwarf galaxies satisfactorily follow the classical Tully-Fisher relation if M_{21} magnitudes are used instead of M_B .

Fig. 5 allows one to estimate the distances of dwarf irregular galaxies with a typical error of $\sigma(\log D) = 0.27$. The scatter of late-type galaxies in Fig. 5 is not a result of measurement errors of W_{50} and S_{HI} , but is due to the irregular shape of dwarfs caused by turbulent motions in them. One would hope that by taking into account the inclination angle (i) of the galaxy's rotation axis with respect to the line of sight, the dispersion in the M_{21} vs. W_{50} diagram could be reduced. If the galaxy has the shape of an ellipsoid of rotation with a true axial ratio $(b/a)_0$ and an apparent axial ratio b/a , then the correction of W_{50} for the inclination is expressed as

$$W_{50}^c = W_{50} / \sin i, \quad (12)$$

where

$$\sin^2 i = \frac{1 - (b/a)^2}{1 - (b/a)_o^2}. \quad (13)$$

Since the typical axial ratio for irregular dwarfs is $(b/a)_o = 0.6$ (Roychowdhury et al. 2013; Karachentsev et al. 2017), the correction for inclination takes the form

$$W_{50}^c = \frac{0.80 W_{50}}{\sqrt{1 - (b/a)^2}}. \quad (14)$$

The bottom panel of Fig. 5 exhibits the distribution of irregular dwarfs by M_{21} and W_{50}^c after accounting the correction for their inclination angle. Taking into account the inclination does not reduce the dispersion, but instead slightly increases it. The probable cause for the scatter is the difference in the shape of irregular dwarfs from the ellipsoid of rotation, especially in relation to the shape of their gas component (Roychowdhury et al. 2010).

In Karachentsev et al. (2017) the gaseous Tully-Fisher relation have been studied for 206 LV galaxies. The regression line for their distribution over hydrogen mass and HI line width W_{50} has a slope of 2.08 and $\sigma(\log M_{\text{HI}}) = 0.43$. Passing from W_{50} to W_{50}^c leaves the regression slope and the dispersion nearly the same. In the current study, no regression was performed, instead we used the classical Tully-Fisher relation (11)

⁵ Between “the absolute HI magnitude” M_{21} and mass M_{HI} there is the equality $\log(M_{\text{HI}}) = 2.33 - 0.4M_{21}$.

with slope of 2.91 which gives $\sigma(\log M_{\text{HI}}) = 0.54$ for our data. The difference in the slope is negligible, especially considering that our range of widths is much smaller (by a factor of 5), and that the slope is probably flattened by high-mass galaxies. It can be seen from figure 9 in Karachentsev et al. (2017) that the dispersion increases appreciably while passing from massive spirals to dwarfs especially for galaxies with $W_{50} \lesssim 30 \text{ km s}^{-1}$: there is a noticeable deficit of HI mass in this region compared to the regression line. The majority of the galaxies in our sample are in this region, resulting in a larger dispersion.

Our radial velocity measurements led to the discovery of some dwarf galaxies probably associated with the bright LV spirals: NGC 628, NGC 2787, NGC 3556, NGC 4490, NGC 4594, and NGC 5055. The 4 new supposed satellites around their host galaxies: NGC 2787, NGC 3556, NGC 4490 and NGC 5055 have a mean linear projected separation of 159 kpc and a mean-square radial velocity difference of 57 km s^{-1} with respect to their hosts giving the average total-mass-to-K-band luminosity of the spiral galaxies to be (6.9 ± 1.6) in the solar units. Also, four dwarf galaxies (Dw 1234–1142, LV J1235–1104, Dw 1235–1216, and PGC 974136) are likely new members of the group around the most luminous LV galaxy, NGC 4594 (Sombrero).

6. CONCLUSIONS

Our HI survey of 105 nearby late-type dwarf galaxies using the GBT has produced 77 detections (73 % of the sample). The median HI-parameters of the detected galaxies are $S_{\text{HI}} = 0.69 \text{ Jy km s}^{-1}$, $V_{\text{HI}} = 732 \text{ km s}^{-1}$, and $W_{50} = 32 \text{ km s}^{-1}$. About half of them are mem-

bers of the Local Volume having kinematic distances $D_{\text{NAM}} < 12 \text{ Mpc}$ and low hydrogen masses in the range of $\log(M_{\text{HI}}/M_{\odot}) = [5.57\text{--}9.14]$. Most of the detected dwarfs are gas-dominated objects with the median gas-to-stellar mass ratio of 1.87. In general, the dwarf galaxies follow the classic Tully-Fisher relation, obtained for large disk-dominated spiral galaxies, if their m_{21} magnitudes are used instead of B-magnitudes. This allows one to make rough estimates of the distances of gas-rich dwarfs with a typical error of $\sigma(\log D) \sim 0.27$.

Among the remaining 28 undetected galaxies, most are Tr-type galaxies (transition between dSph and Irr). This category of dwarfs is distinguished by a fairly smooth structure, redder $B - V$ color index, and a weak UV flux. Five of the 28 undetected targets turned out to be very nearby galaxies, whose HI flux is masked by the bright emission of local hydrogen from the Milky Way.

AEN, IDK, DIM, and MIC are supported by the Russian Science Foundation grant № 24–12–00277.

The National Radio Astronomy Observatory is a facility of the National Science Foundation operated under cooperative agreement by Associated Universities, Inc.

The authors thank Toney Minter for helpful discussions and the GBT operators for ensuring smooth operations during observing sessions.

This work has made use of the DESI Legacy Imaging Surveys (<http://www.legacy/surveys.org/>), the Galaxy Evolution Explorer (GALEX, <http://www.galex.caltech.edu/index.html>), HyperLEDA database (<http://leda.univ-lyon1.fr/>), and the current version of the Local Volume galaxy database (<http://www.sao.ru/lv/lvgdb>).

REFERENCES

- Abazajian, K. N., Adelman-McCarthy, J. K., Agüeros, M. A., et al. 2009, *ApJS*, 182, 543, doi: [10.1088/0067-0049/182/2/543](https://doi.org/10.1088/0067-0049/182/2/543)
- Abbott, T. M. C., Adamów, M., Agüena, M., et al. 2021, *ApJS*, 255, 20, doi: [10.3847/1538-4365/ac00b3](https://doi.org/10.3847/1538-4365/ac00b3)
- Adams, E. A. K., Adebahr, B., de Blok, W. J. G., et al. 2022, *A&A*, 667, A38, doi: [10.1051/0004-6361/202244007](https://doi.org/10.1051/0004-6361/202244007)
- Aihara, H., AlSayyad, Y., Ando, M., et al. 2019, *PASJ*, 71, 114, doi: [10.1093/pasj/psz103](https://doi.org/10.1093/pasj/psz103)
- Anand, G. S., Lee, J. C., Van Dyk, S. D., et al. 2020, *Monthly Notices of the Royal Astronomical Society*, 501, 3621, doi: [10.1093/mnras/staa3668](https://doi.org/10.1093/mnras/staa3668)
- Carlsten, S. G., Greene, J. E., Beaton, R. L., Danieli, S., & Greco, J. P. 2022, *The Astrophysical Journal*, 933, 47, doi: [10.3847/1538-4357/ac6fd7](https://doi.org/10.3847/1538-4357/ac6fd7)
- Casey, K. J., Greco, J. P., Peter, A. H. G., & Davis, A. B. 2023, *MNRAS*, 520, 4715, doi: [10.1093/mnras/stad352](https://doi.org/10.1093/mnras/stad352)
- de Vaucouleurs, G., de Vaucouleurs, A., Corwin, Jr., H. G., et al. 1991, *Third Reference Catalogue of Bright Galaxies*
- Dey, A., Schlegel, D. J., Lang, D., et al. 2019, *AJ*, 157, 168, doi: [10.3847/1538-3881/ab089d](https://doi.org/10.3847/1538-3881/ab089d)
- Giovanelli, R., Haynes, M. P., Kent, B. R., et al. 2005, *AJ*, 130, 2598, doi: [10.1086/497431](https://doi.org/10.1086/497431)
- Haynes, M. P., Giovanelli, R., Kent, B. R., et al. 2018, *ApJ*, 861, 49, doi: [10.3847/1538-4357/aac956](https://doi.org/10.3847/1538-4357/aac956)
- Herrmann, K. A., Hunter, D. A., Zhang, H.-X., & Elmegreen, B. G. 2016, *AJ*, 152, 177, doi: [10.3847/0004-6256/152/6/177](https://doi.org/10.3847/0004-6256/152/6/177)

- Jiang, P., Tang, N.-Y., Hou, L.-G., et al. 2020, *Research in Astronomy and Astrophysics*, 20, 064, doi: [10.1088/1674-4527/20/5/64](https://doi.org/10.1088/1674-4527/20/5/64)
- Karachentsev, I. D., Chazov, M. I., & Kaisin, S. S. 2025, *MNRAS*, 537, L21, doi: [10.1093/mnrasl/slae111](https://doi.org/10.1093/mnrasl/slae111)
- Karachentsev, I. D., & Kaisina, E. I. 2022, *Astrophysical Bulletin*, 77, 372, doi: [10.1134/S1990341322040058](https://doi.org/10.1134/S1990341322040058)
- Karachentsev, I. D., Kaisina, E. I., & Kashibadze (Nasonova), O. G. 2017, *AJ*, 153, 6, doi: [10.3847/1538-3881/153/1/6](https://doi.org/10.3847/1538-3881/153/1/6)
- Karachentsev, I. D., Karachentseva, V. E., Kaisin, S. S., & Kaisina, E. I. 2024a, *Astrophysics*, 66, 441, doi: [10.1007/s10511-024-09801-w](https://doi.org/10.1007/s10511-024-09801-w)
- Karachentsev, I. D., Karachentseva, V. E., Kaisin, S. S., & Zhang, C.-P. 2024b, *A&A*, 684, L24, doi: [10.1051/0004-6361/202449672](https://doi.org/10.1051/0004-6361/202449672)
- Karachentsev, I. D., Makarov, D. I., & Kaisina, E. I. 2013, *AJ*, 145, 101, doi: [10.1088/0004-6256/145/4/101](https://doi.org/10.1088/0004-6256/145/4/101)
- Karachentsev, I. D., Makarova, L. N., Tully, R. B., Rizzi, L., & Shaya, E. J. 2018, *The Astrophysical Journal*, 858, 62, doi: [10.3847/1538-4357/aabaf1](https://doi.org/10.3847/1538-4357/aabaf1)
- Karachentseva, V. E., Karachentsev, I. D., Kaisina, E. I., & Kaisin, S. S. 2023, *A&A*, 678, A16, doi: [10.1051/0004-6361/202347085](https://doi.org/10.1051/0004-6361/202347085)
- Koribalski, B. S., Staveley-Smith, L., Kilborn, V. A., et al. 2004, *AJ*, 128, 16, doi: [10.1086/421744](https://doi.org/10.1086/421744)
- Kourkchi, E., Courtois, H. M., Graziani, R., et al. 2020, *AJ*, 159, 67, doi: [10.3847/1538-3881/ab620e](https://doi.org/10.3847/1538-3881/ab620e)
- Kovač, K., Oosterloo, T. A., & van der Hulst, J. M. 2009, *MNRAS*, 400, 743, doi: [10.1111/j.1365-2966.2009.14662.x](https://doi.org/10.1111/j.1365-2966.2009.14662.x)
- Lee, M. G., Freedman, W. L., & Madore, B. F. 1993, *ApJ*, 417, 553, doi: [10.1086/173334](https://doi.org/10.1086/173334)
- Makarov, D., Prugniel, P., Terekhova, N., Courtois, H., & Vauglin, I. 2014, *A&A*, 570, A13, doi: [10.1051/0004-6361/201423496](https://doi.org/10.1051/0004-6361/201423496)
- Roychowdhury, S., Chengalur, J. N., Begum, A., & Karachentsev, I. D. 2010, *MNRAS*, 404, L60, doi: [10.1111/j.1745-3933.2010.00835.x](https://doi.org/10.1111/j.1745-3933.2010.00835.x)
- Roychowdhury, S., Chengalur, J. N., Karachentsev, I. D., & Kaisina, E. I. 2013, *MNRAS*, 436, L104, doi: [10.1093/mnrasl/slt123](https://doi.org/10.1093/mnrasl/slt123)
- Sardone, A., Pisano, D. J., Pingel, N. M., et al. 2021, *ApJ*, 910, 69, doi: [10.3847/1538-4357/abde45](https://doi.org/10.3847/1538-4357/abde45)
- Shaya, E. J., Tully, R. B., Hoffman, Y., & Pomarède, D. 2017, *ApJ*, 850, 207, doi: [10.3847/1538-4357/aa9525](https://doi.org/10.3847/1538-4357/aa9525)
- Tanaka, M., Ikeda, H., Murata, K., et al. 2021, *PASJ*, 73, 735, doi: [10.1093/pasj/psab034](https://doi.org/10.1093/pasj/psab034)
- Tully, R. B., & Fisher, J. R. 1977, *A&A*, 54, 661
- Tully, R. B., Shaya, E. J., Karachentsev, I. D., et al. 2008, *ApJ*, 676, 184, doi: [10.1086/527428](https://doi.org/10.1086/527428)
- Šiljeg, B., Adams, E. A. K., Fraternali, F., et al. 2024, *A&A*, 692, A217, doi: [10.1051/0004-6361/202449923](https://doi.org/10.1051/0004-6361/202449923)
- Willmer, C. N. A. 2018, *ApJS*, 236, 47, doi: [10.3847/1538-4365/aabfdf](https://doi.org/10.3847/1538-4365/aabfdf)
- Zhang, C.-P., Zhu, M., Jiang, P., et al. 2024, *Science China Physics, Mechanics, and Astronomy*, 67, 219511, doi: [10.1007/s11433-023-2219-7](https://doi.org/10.1007/s11433-023-2219-7)